ACI STRUCTURAL JOURNAL TECHNICAL PAPER

Title No. 111-S03

Comparison of Moment-Curvature Models for Fiber-Reinforced Polymer Plate-End Debonding Studies Using Global Energy Balance Approach

by Garfield X. Guan and Chris J. Burgoyne

This paper compares a number of different moment-curvature models for cracked concrete sections that contain both steel and external fiber-reinforced polymer (FRP) reinforcement. The question of whether to use a whole-section analysis or one that considers the FRP separately is discussed. Five existing and three new models are compared with test data for moment-curvature or load deflection behavior, and five models are compared with test results for plate-end debonding using a global energy balance approach (GEBA). A proposal is made for the use of one of the simplified models.

The availability of a simplified model opens the way to the production of design aids so that the GEBA can be made available to practicing engineers through design guides and parametric studies.

Keywords: energy release rate; global energy balance approach; moment-curvature model; plate-end debonding; whole section treatment.

INTRODUCTION

Fiber-reinforced polymer (FRP) plates are widely used to strengthen reinforced concrete (RC) beams under the circumstances of deterioration, aging, change of functions or loads, or to match upgraded code requirements, but plate-end (PE) debonding is recognized as a common failure mode that has proved difficult to analyze reliably. PE debonding due to failure of the adhesive layer or at the concrete-adhesive interface can now be prevented by using the proper techniques and the correct adhesive.[1] Most of the remaining problems occur when a relatively thick layer of concrete breaks off, together with the FRP plate.[2-4] Thus, fracture of concrete in the beam cover layer is important, and fracture studies have been adopted for debonding analysis.[5-10] Most of the existing fracture analyses focus on the details of local fracture, but recently the global energy balance approach (GEBA) has been developed by Achintha and Burgoyne[10-13] and others.[14,15] GEBA works by equating the energy released when a crack forms with the energy needed to form the crack.[10,13] A key component of these analyses is the moment curvature (M-κ) relationship for a beam that has both steel and FRP reinforcement, and is a partially cracked FRP. The method used in References 10-13 uses a Branson-type analysis for the concrete and steel elements of the beam, which are subjected both to the external load and the reaction to the force in the FRP. The calculations required in this method were complicated, however, which means that it is difficult to apply to design or parametric studies. This paper proposes simplified methods for calculating the M-κ relationship with comparable accuracy. This enables the development of design tools.

RESEARCH SIGNIFICANCE

The study presented herein compares various moment-curvature (M-κ) relationships for the global energy balance approach (GEBA) to determine the load at which an FRP plate will debond from a RC beam. The core of GEBA is the M-κ relationship, which was complex as first adopted in GEBA,[10-13] and made GEBA inconvenient for practice. Various M-κ relationships for deflection estimation are available, but their suitability for GEBA use is unknown. This work examines the suitability of various M-κ models for debonding analysis. Comparison between various existing and proposed M-κ models shows that conventional whole section M-κ models with simple modifications can provide comparable accuracy to complicated models. Although further efforts are required to calibrate an M-κ relationship, particularly for the concern of debonding analysis, this study points out the crucial features in an M-κ relationship.

GEBA DEBONDING ANALYSIS WITH WHOLE SECTION TREATMENT

PE debonding normally occurs close to the supports under a low flexural load. The beam sections are almost not yielding, and respond to bending in a linearly-elastic manner. Hence, the continuum energy is mainly the elastic strain energy E_{strain}. Thus, the energy released by fracture is obtained by subtracting the change in strain energy ΔE_{strain} from the external work W_{ext} during the fracturing process. The change in strain energy and the external work done on a section can be obtained by comparing the moment-curvature (M-κ) response of this section in intact and fractured states. Figure 1 shows the M-κ response of a beam section (Section A) before yielding in intact and fractured states. The section strain energy $E_{strain\text{-}A}$ in the intact and fractured states is represented by triangles OPD and OQC, respectively. Because debonding is a sudden process, the moment due to the external load in a determinate system $M_{ext\text{-}A}$ remains constant, but the curvature increases as the fractured beam becomes softer and deflects further, so that the external work done on the section $W_{ext\text{-}A}$ is represented by the rectangle PQCD. Furthermore, the conventional cracks (flexural and shear cracks) are assumed not to change during the sudden debonding process; therefore, the shaded areas OEP

ACI Structural Journal, V. 111, No. 1, January-February 2014.
MS No. S-2011-280.R3 was received July 29, 2013, and reviewed under Institute publication policies. Pertinent discussion including author's closure, if any, will be published ten months from this journal's date if the discussion is received within four months of the paper's print publication.

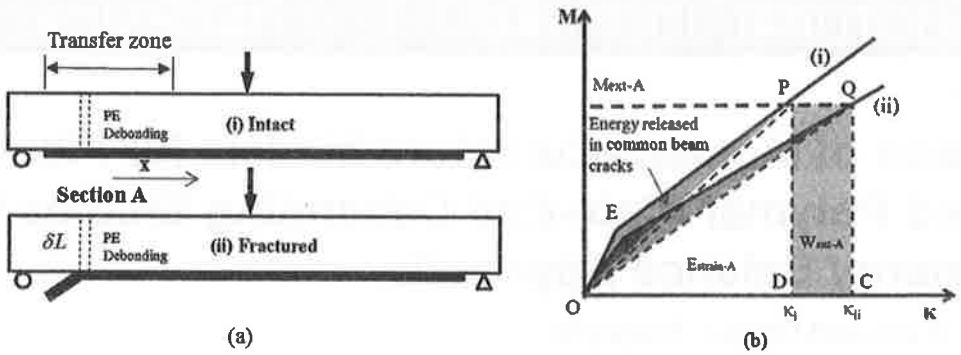

Fig. 1—Comparison of moment-curvature state of intact section (i) and fractured section (ii).

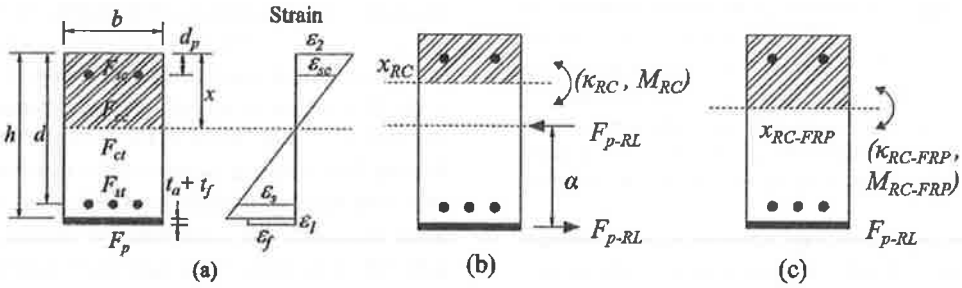

Fig. 2—(a) Typical section; (b) whole section treatment; and (c) separate section treatment.

and OFQ, which denote the energy goes to these cracks are assumed the same in both states. Thus, the energy released from Section A to the debonding fracture is $W_{ext\text{-}A} - \Delta E_{strain\text{-}A}$.

The degree of bond between the FRP and the concrete is important. When the FRP is completely debonded its force has to be zero. When it is fully bonded, its force can be determined from a section analysis that satisfies compatibility. The force has to build up through a transfer zone.[10,16] Achintha and Burgoyne showed that this zone extends for approximately 30 times the FRP plate thickness ($30t_f$) from the debonding point (Fig. 1(a)).[11] Only beam sections within the transfer zone contribute to the energy release[10,16] because the state in the rest of the beam does not alter. Thus, the overall energy available to release can be obtained by summing the energy contribution from these sections, and is expressed in terms of energy release rate per unit fracture area as $G_R = (W_{ext} - \Delta E_{strain})/(b \times \delta L)$, where b is the beam width, and δL is the debonding fracture length.

Within the transfer zone, the FRP plate and RC beam are only partially bonded, meaning the FRP-RC section is not strictly planar, and its strain is not compatible with the bottom concrete (Fig. 2(a)), but it is necessary to model it because this is where the flexural strain energy is absorbed. This partially bonded condition can be treated either using an M-κ model for the whole FRP-RC section but with the real FRP force predetermined, as shown in Fig. 2(b), or by separating the FRP plate and the RC section and using an M-κ model to describe the RC section under a predetermined FRP force, as shown in Fig. 2(c).

The separate-section treatment (Fig 2(c)) was used by Achintha and Burgoyne.[10-11] The objective was to use a Branson-type model to determine the curvature in the RC beam under a given loading, but it was recognized that Branson's method was developed for singly reinforced RC sections with no axial load. It was unreasonable to use the same formula for a beam with two different reinforcing materials at two levels. Thus, the FRP was considered as a separate element, and the Branson model needed to be modified to account for the axial force. The test results for beams subject to both moment and axial load by Sakai and Kakuta[17] were used to determine where the resulting axial force should be applied. The strain energy is also spread over three terms as the flexure in the RC section plus axial effects in both the RC and FRP, which brings further complications. The objective of the present work is to find simplified ways of determining the M-κ relationship for a beam with both steel and FRP so that the strain energy can be determined.

The present analysis still requires knowledge of the real force in the FRP in the transfer zone $F_{p\text{-}RL}$. The real FRP force is considered relating to the fully bonded FRP force as shown in Fig. 3, where the x-axis shows the distance from the plate end. An analysis is first carried out on the assumption that the FRP is fully bonded, so plane sections remain plane, giving the fully bonded FRP force $F_{p\text{-}FB}$. An exponential expression that describes the relationship between $F_{p\text{-}RL}$ and $F_{p\text{-}FB}$ in the transfer zone can then be used to determine $F_{p\text{-}RL}$.[10,16] The difference between the two forces shown in Fig. 3 can be expressed by Eq. (1)

$$F_{p\text{-}RL}(x) = F_{p\text{-}FB}(x) - F_{p0} \times e^{-\lambda\sigma} \quad (1)$$

where $F_{p\text{-}RL}(x)$ and $F_{p\text{-}FB}(x)$ are the partially and fully bonded FRP forces; x is the distance between the section and the plate end, which is smaller than $30t_f$, and $\lambda = \sqrt{G_a / (t_a E_f t_f)}$ which indicates that if a softer and thicker adhesive and a stiffer and thicker FRP plate are used, a larger difference is expected between $F_{p\text{-}FB}$ and $F_{p\text{-}RL}$.

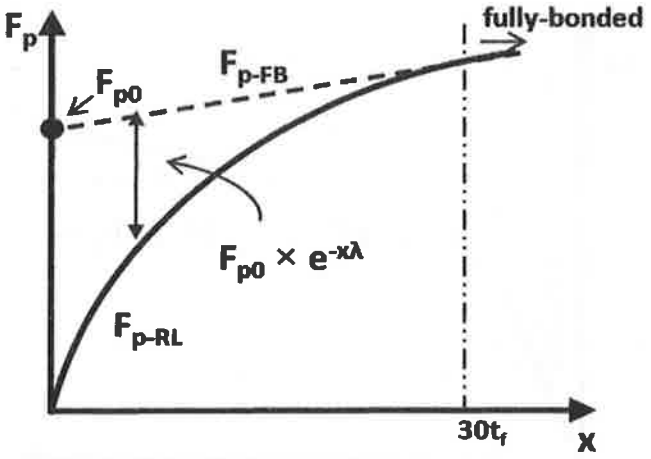

Fig. 3—Relationship between fully bonded and real FRP force.

A step-by-step GEBA debonding analysis with whole-section treatment is as follows:

1. Analyze the FRP-RC section under a fully bonded condition using an appropriate M-κ model to determine F_{p-FB};
2. Calculate F_{p-RL} in the transfer zone from F_{p-FB} using Eq. (1) for the beam in both the intact and fractured states;
3. Analyze the FRP-RC section as a whole using the same M-κ model as in Point 1, for both the intact and fractured states with the real F_{p-RL}, which indicates smaller strains at the FRP plate than at the bottom fiber of the RC section; and
4. Determine the energy release rate as explained in Fig. 1 ($G_R = (W_{ext} - \Delta E_{strain})/(b \times \delta L)$).

The key to this procedure is the choice of M-κ relationship.

M-κ MODELS FOR GEBA ANALYSIS

Various M-κ models are available for RC beams from codes and the literature, most of which are based on Branson's model that use empirical interpolations to describe partially cracked sections. With the increasing application of FRP plate in retrofitting, M-κ models for FRP-RC beams have also been developed,[18-20] and a detailed review can be found in Reference 21. By comparing the external moment M_{ext} with the moments at the states of first cracking of concrete in tension κ_{cr}, M_{cr}; first yield of tension steel κ_y, M_y; and ultimate state (at concrete crushing) κ_{ult}, M_{ult}, an M-κ model for FRP-RC beam usually classifies beam sections as uncracked ($M_{ext} \le M_{cr}$), partially cracked ($M_{cr} \le M_{ext} \le M_y$), and fully cracked ($M_y \le M_{ext} \le M_{ult}$), respectively.

Conventionally, M-κ models were used to predict *overall* beam deflection for checking serviceability criteria, and only needed to be accurate when integrated over the whole beam. The current application, however, requires that the M-κ model predicts the *local* bending behavior κ and strain energy E_{strain} for a more complicated section. Different M-κ models are now examined for their potential for GEBA use.

Existing M-κ models

Branson's original model (adopted in ACI 318)[22,23] was designed for RC beams, which were classified only as uncracked and cracked. The M-κ relation is as expressed in Eq. (2)

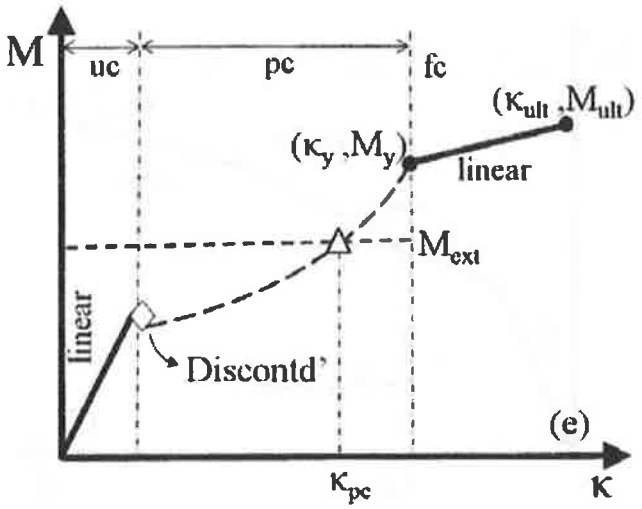

Fig. 4—El-Mihilmy and Tedesco's M-κ *model.*

$$\kappa = \frac{M_{ext}}{E_c I_e} \tag{2}$$

where $I_e = I_g$ (for $M_{ext} \le M_{cr}$), and

$$I_e = \left(\frac{M_{cr}}{M_{ext}}\right)^3 I_g + \left(1 - \left(\frac{M_{cr}}{M_{ext}}\right)^3\right) I_y \quad (\text{for } M_{ext} > M_{cr})$$

where I_g and I_y are the uncracked and fully cracked (computed at first yield) second moments of area. In the present work, when calculating I (the second moment of area), the FRP plate is treated in the same way as steel reinforcement.

Unlike conventional RC beams, an FRP-RC beam can pick up more load even after first yield of the tension steel. Various models have been proposed for this.

El-Mihilmy and Tedesco[19] assumed that the fully cracked M-κ response is a straight line connecting the first-yield state (κ_y, M_y) and the ultimate state (κ_{ult}, M_{ult}), as shown in Fig. 4. They noted that the M-κ response in the partially cracked (κ_{pc}) region is governed more by the first yield state than the first crack state; thus, the Branson's original model was modified to be

$$I_e = I_y \left(1 + \left(1 - \frac{M_{ext}}{M_y}\right)^3\right) \text{ for } M_{cr} \le M_{ext} \le M_y \tag{3}$$

As shown in Fig. 4, where the triangle represents the M-κ state for a partially cracked section, interpolating using information from the first yield state only causes a discontinuity at the first cracking load, this can cause problems for use in GEBA.

Charkas et al.[20] proposed a model for FRP-RC beams in which a simple trilinear M-κ response connected the origin (0,0), the first crack (κ_{cr}, M_{cr}), the first yield (κ_y, M_y), and the ultimate states (κ_{ult}, M_{ult}), as shown in Fig. 5. This model has the advantage of simplicity; only three points are required,

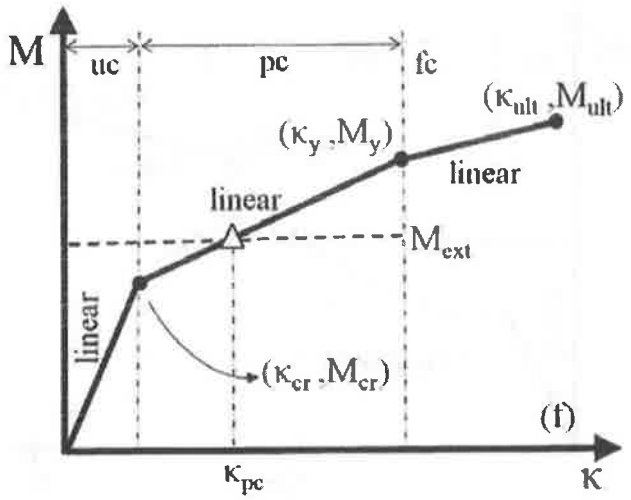

Fig. 5—Charkas et al. M-κ *model*

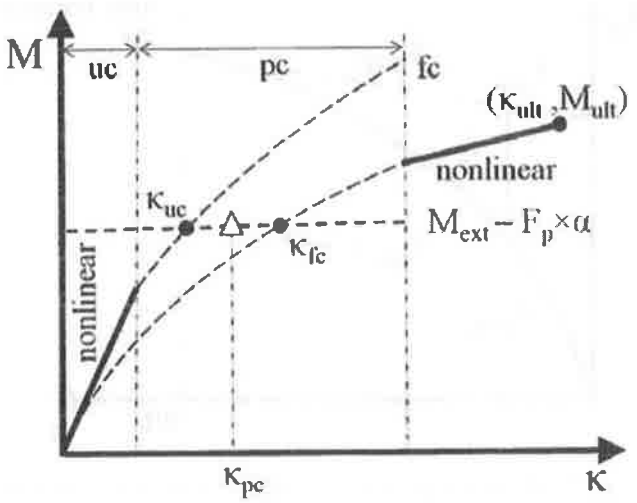

Fig. 6—Achintha and Burgoyne's M-κ *model.*

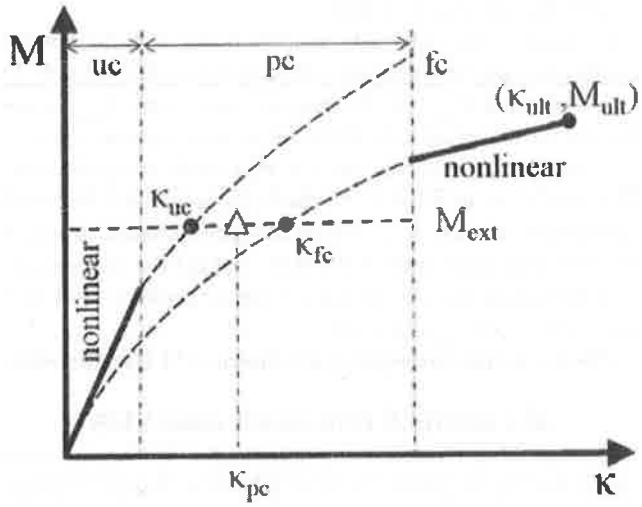

*Fig. 7—*M-κ *Model M1.*

and can capture the post-yielding response. In GEBA, the M-κ pair for the three states should be calculated for each section in both the intact and fractured beams. It will be shown, however, that a curved expression for the partially cracked section is needed to give an accurate estimate of the strain energy.

Achintha and Burgoyne's model[11] gives more complex expressions; it was especially designed for GEBA use. The FRP plate and the RC section are treated separately using an empirical expression to decouple the FRP force. The moment to be resisted by the RC section is then given by $M_{ext} - F_p \times \alpha$, where α is the predetermined moment arm, as shown in Fig. 2(c). Nonlinear expressions are used to determine the uncracked and fully cracked behavior at any load level, and a nonlinear interpolation is made between the two for partially cracked section (Fig. 6). The resulting calculations are complex and iterative.[11] It is proposed that treating the FRP-RC section as a whole can greatly simplify GEBA analysis; thus, whole-section M-κ models are proposed.

Proposed model one (M1)—This model uses the same section analysis as that for the RC part (with moment $M_{ext} - F_p \times \alpha$) in Achintha and Burgoyne's model, and the same interpolation formula, but does not decouple the force in the FRP; calculations can now be carried out with the full external moment M_{ext} applied to the section (Fig. 7), so there is no need to predetermine the moment arm (α in Fig. 2(c)).

The procedures are the same as in Achintha and Burgoyne's model, but the equilibrium equation used is now for the whole section as in Eq. (4)

$$\begin{cases} \sum F_{FRP-RC}(\varepsilon_1, \varepsilon_2) = 0 \\ \sum M_{FRP-RC}(\varepsilon_1, \varepsilon_2) = M_{ext} \end{cases} \quad (4)$$

where ε_1 and ε_2 are the strain at top and bottom concrete fibers, respectively. The curvature of uncracked and fully cracked sections can be solved directly. The effective stiffness of a section is then calculated as

uncracked and fully cracked sections:

$$(EI) = M_{ext}/\kappa \quad (5)$$

Note that E and I are not calculated separately; the effective stiffness EI is a single variable. The same interpolation as in Achintha and Burgoyne's model is used for partially cracked sections, which gives

$$(EI)_{pc} = K_p(EI)_{uc} + (1 - K_p)(EI)_{fc} \quad (6)$$

where $(EI)_{uc}$ and $(EI)_{fc}$ correspond to the curvature obtained from solving the partially cracked sections as if it were uncracked and fully cracked; and

$$K_p = \left(\frac{M_{cr}}{M_{ext}}\right)^4 \left(1 - \left(\frac{M_{ext} - M_{cr}}{M_y - M_{cr}}\right)^4\right)$$

is the interpolation coefficient to ensure the M-κ curve is continuous at first crack (κ_{cr}, M_{cr}) and first yield (κ_y, M_y).

Model M1 reduces the uncertainty due to the selection of the decoupling moment arm (α); however, as done Achintha

and Burgoyne's model, calculations should be performed for each section in the transfer zone. This leads to a large amount of computation because iteration is required for solving nonlinear Eq. (4).

Proposed model two (M2)—This model is the same as M1, except that the effective moment of inertia I_e instead of the effective stiffness (EI = M/κ) is used for partially cracked section interpolation (Eq. (7))

$$I_{e\text{-}pc} = K_p I_{e\text{-}uc} + (1 - K_p) I_{e\text{-}fc} \quad (7)$$

Because the section where PE debonding is likely to occur is near the plate end and under low loads, the concrete should behave almost elastically so that the Young's modulus can be taken as a constant. Thus, it is sufficient to interpolate on I_e. In the transfer zone, where the FRP is not fully bonded, the area of the FRP is reduced by the ratio $F_{p\text{-}RL}/F_{p\text{-}FB}$ (Fig. 3) when calculating $I_{e\text{-}uc}$ and $I_{e\text{-}fc}$. Comparing the results from M1 and M2 will give an estimation of the influence of the section nonlinearity.

Proposed model three (M3)—This model synthesizes the above ideas to simplify the GEBA formulation while keeping the important features (continuity at the cracking and yielding points), as shown in Fig. 8. Because most of the sections of interest (in the transfer zone) are partially cracked, the uncracked and fully cracked sections are of less importance, and linear expressions are used. To reduce the times for solving Eq. (4), which is solved for each section in M1 and M2, the interpolation for partially cracked sections is carried out between the moment of inertia at the first-crack $I_{e\text{-}cr}$ (ε_1 is known) and the first-yield $I_{e\text{-}y}$ (strain in the steel ε_s is known). The interpolation is shown in Eq. (8)

$$I_{e\text{-}pc} = K_p I_{e\text{-}cr} + (1 - K_p) I_{e\text{-}y} \quad (8)$$

Comparison of M-κ models with experiments

The M-κ models can be tested in two ways: first, by comparing the predictions of the model for the curvatures, strains and deflections; and second, by comparing the predictions for the debonding load. The first is discussed in this section.

Hognestad's parabolic stress-strain expression[24] and ACI code[23] are adopted, giving the concrete elastic modulus as $E_c = 4733\sqrt{f_c'}$ N/mm^2 ($E_c = 57{,}000\sqrt{f_c'}$ psi), the tensile strength as $f_t = 0.62\sqrt{f_c'}$ N/mm^2 ($f_t = 7.5\sqrt{f_c'}$ psi), the ultimate compressive strain as 0.003, and the ultimate tensile strain as f_t/E_c.

Table 1 lists a number of tests[25-32] that have been carried out over the years to investigate the debonding behavior of beams with FRP, but the same papers include sufficient details to allow the pre-debonding moment curvature responses to be determined. All of these tests are four-point bending with equal shear spans, and a collective description is given in References 12 and 25 to 32. In GEBA, the ability to estimate the local bending response is of utmost importance, so where possible, the M-κ and load-strain relationships are plotted. The strain is obtained by assuming that the section is fully bonded because debonding has not yet occurred, and the sections being considered are away from the plate ends. When only the load-deflection relationship is available, predictions are made by integrating section curvatures to provide deflections.

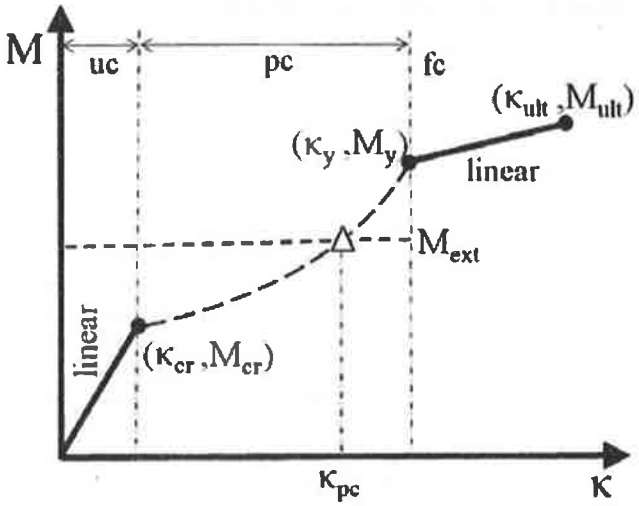

Fig. 8—M-κ *Model M3.*

The comparisons for several different tests using all the possible M-κ relationships are shown in Fig. 9. In addition to the various models described previously, comparisons have also been made using the model adopted by Eurocode 2004 (EC2).[33] In general, the ACI model is not designed to predict the post-yield behavior, so it departs from other models after steel yields. A negligible variation can be seen at the first crack, mainly because M1 and Achintha and Burgoyne's model use effective stiffness, while others use second moment of area. The major difference between the models is within the partially cracked region, which is critical for GEBA analysis.

Figure 9(a) shows the results of a test carried out by Spadea specifically to measure the moment-curvature relationship.[27] The measured curvature is consistently higher than the predictions, and the measured yield moment is higher than the predictions, but there is very little difference between the various models. The quoted steel strength is 435 MPa (63.1 ksi), but the predictions for the yield moment only match if f_y is taken as 530 MPa (76.9 ksi). Because the onset of yield is clearly observed, and the predictions rely only on simple beam theory, which is known to be very accurate, the conclusion is that the quoted value is a nominal one, rather than a measured one. Similarly, the stiffness match if E_c is taken as 20 GPa (2901 ksi) rather than 24 GPa (3481 ksi), which is the value obtained from the quoted concrete cylindrical strength 24 MPa (3.5 ksi).

Figure 9(b) shows comparisons with tests by Arduini[30]; these measure FRP strain rather than curvature and are related primarily to the partially cracked state. The steel did not yield in these tests. There is considerable scatter in the predictions; the ACI, M2, and M3 predictions lie below the test results soon after cracking (that is, the predicted strains are higher for a given load). It is likely that the places where the strains are measured are away from the major mid-span cracks just after the first cracking stage. The EC2 and

Table 1—List of data for validation

Reference	Beam specimen	Failure load, kN	Plate material	L_{span}, mm	L_{shear}, mm	Aggregate size, mm/type	L_{rl}, mm	b_b, mm	h_b, mm	c_b, mm	d_c, mm	A_c, mm²	A_{sl}, mm²	f'_c, MPa	f_{cu}, MPa	f_{350}, MPa	t_p, mm	A_f, mm²	E_p, GPa	l_{ad}, mm	E_a, GPa	Failure mode
Ross et al.[25]	G2*	83.1	CFRP	2742	914	—	0	200	200	48	20†	259	142	54.8	411	410	0.45	91.4	138	2†	—	Debond
	G5*	146.4	CFRP	2742	914	—	0	200	200	48	20†	612	142	54.8	410	410	0.45	91.4	138	2†	—	Crush
Alagusundaramoorthy et al.[26]	CB3 and 4-2S*	260	CFRP	4576	1830	—	153	230	380	50	29.5	981.8	127	29.5	414	414	1.4	212.8	138	3	—	Crush
	CB5-3S*	287	CFRP	4576	1830	—	153	230	380	50	29.5	981.8	127	29.5	414	414	1.4	319.2	138	3	—	Crush
Spadea et al.[27]	A3.1*	74.8	CFRP	4800	1800	—	50	140	300	33	33	402	402	24	435	435	1.2	96	152	2	—	Debond
Li et al.[28]	A*	96	CFRP	1100	400	16 (crushed)	30	130	200	35	35†	101	101	37	530†	530†	1.3	120	120	2†	—	—
Ahmed[29]	AF2	83	CFRP	—	500	16 (crushed)	**200**	125	225	25	25	100.5	57	41	568	568	0.33	41	240	2	8†	Debond
	AF3	96.6	CFRP	—	500	16 (crushed)	**100**	125	225	25	25	**100.5**	57	41	568	568	0.33	41	240	2	8†	Debond
	CF2-1	104.8	CFRP	—	500	16 (crushed)	100	125	225	25	25	**128.8**	57	43	568	568	0.33	41	240	2	8†	Debond
	CF3-1	118	CFRP	—	500	16 (crushed)	100	125	225	25	25	**150.8**	57	43	568	568	0.33	41	240	2	8†	Debond
	CF4-1	140	CFRP	—	500	16 (crushed)	100	125	225	25	25	**207.3**	57	43	568	568	0.33	41	240	2	8†	Debond
Arduini et al.[30]	A4	110	CFRP	2000	700	10 (rounded)†	150	200	200	37	37	308	308	31	540	540	1.3	**195**	167	2†	11	Debond
	A5	86	CFRP	2000	700	10 (rounded)†	150	200	200	37	37	308	308	31	540	540	1.3	**390**	167	2†	11	Debond
	A6*	115	CFRP	2000	700	—	150	200	200	37	37	308	308	31	540	540	1.3	390	167	2†	11	Anchor
Fanning and Kelly[31]	F3 and F4	101.5	CFRP	2800	100	20 (crushed)†	**385**	155	240	37	37	339	226	80	530	530	1.2	144	155	3	6†	Debond
	F9 and F10	72.0	CFRP	2800	100	20 (crushed)†	**550**	155	240	37	37	339	226	80	530	530	1.2	144	155	3	6†	Debond
Nguyen et al.[32]	A1100	57.3	CFRP	1330	440	20 (crushed)†	**115**	120	150	25	25	235.5	57	32.1	384	384	1.2	96	181	1.5	13	Debond
	A1150	58.9	CFRP	1330	440	20 (crushed)†	**90**	120	150	25	25	235.5	57	32.1	384	384	1.2	96	181	1.5	13	Debond

*Tests for load-deformation relationship comparison only.

†Assumed.

Notes: 1 mm = 0.039 in.; 1 mm² = 0.00155 in.²; 1 kN = 0.225 kip; 1 MPa = 0.145 ksi; 1 GPa = 145 ksi.

El-Mihilmy and Tedesco predictions underestimate the strain for most of the post-cracking region.

Figure 9(c) also shows predictions of strain, and relate to tests by Li et al.[28] Cracking was predicted at lower loads than was observed, but it is possible that this was due to the strain gauge not being located near one of the first cracks. In general, all the curves are reasonable apart from EC2 and Charkas et al. predictions, which underestimate the strain.

Figure 9(d) relates to tests by Alagusundaramoorthy et al.[26] These show unexpected measurements of strain, which are probably related to the proximity of cracks to the strain gauge locations. As before, Charkas et al. and EC2 predictions underestimate the strains. Figure 9(e) relates to a different gauge at mid-span for the same beam, and shows more consistent results. Figures 9(f) and (g) show deflection predictions for different beams by the same author, and show good agreement for all models. Finally, Fig. 9(h) shows deflections in tests carried out by Ross et al.[25]; they show good agreement with all models except for the ACI curve in the post-yielding region, for which it was not intended.

In general, the deflection predictions for all models are good, probably because deflections are obtained by integrating the curvatures, which tends to average out the errors. Predictions of strains are less consistent, because the strain data obtained from tests are influenced by the local cracking patterns, while the models assume that the effects of the cracks are smeared. Furthermore, there is very little test data for curvatures. It can be concluded that the EC2, Charkas et al., and El-Mihilmy and Tedesco models are less reliable than the others in predicting partially cracked behavior.

A deflection prediction is required in GEBA to find the external work W_{ext} done during debonding. It is possible for beam sections in the middle region to yield; therefore, knowledge about the post-yielding behavior is required. Models that purely adopt Branson's method, such as ACI, do not cover this state. The EC2 model appeared to agree less with the tests than the others, and will not be considered further. Many of the sections in the transfer zone (close to plate end) are likely to be at or near the first crack state, where the effect of the discontinuity in El-Mihilmy and Tedesco's model will be crucial; thus, is not suitable for GEBA use.

COMPARISON OF GEBA RESULTS WITH EXPERIMENTS

Having compared the various M-κ models with tests, it is now possible to investigate which ones give the best predictions in a GEBA analysis. Due to space limitations, the comparison presented is limited to a small number that cover a range of different geometric and material properties. These tests are listed in Table 1. Those parameters that are changed in each set of tests is highlighted in bold and with underline.

PE debonding depends on both the load and the location of the plate end.[12,13] A comparison of the GEBA prediction with tests is carried out using a plot in Fig. 10. The x-axis denotes the ratio of the predicted debonding load (P) to the real debonding load P_{peak}, with a deviation of 10%. The y-axis is the difference between the predicted debonding location L_p (the distance from the debonded plate end to the beam support) and the real plate end L_{rl}, normalized by the concrete cover thickness c. $L_p - L_{rl}$ has no meaning if it is negative. PE debonding is commonly initiated by shear cracks within the concrete cover having an angle of approximately 45 degrees,[12,13] so the effective position of the plate end has an uncertainty of approximately one cover thickness.

The position of the data points (triangles) is determined by the possible combination of the plate end location and structural load such that the energy release rate G_R is equal to the fracture energy G_f. Because fracture energy can be expected to vary locally, the effect of ±10% variation in G_f is shown by the error bars on the data points. Debonding is inherently

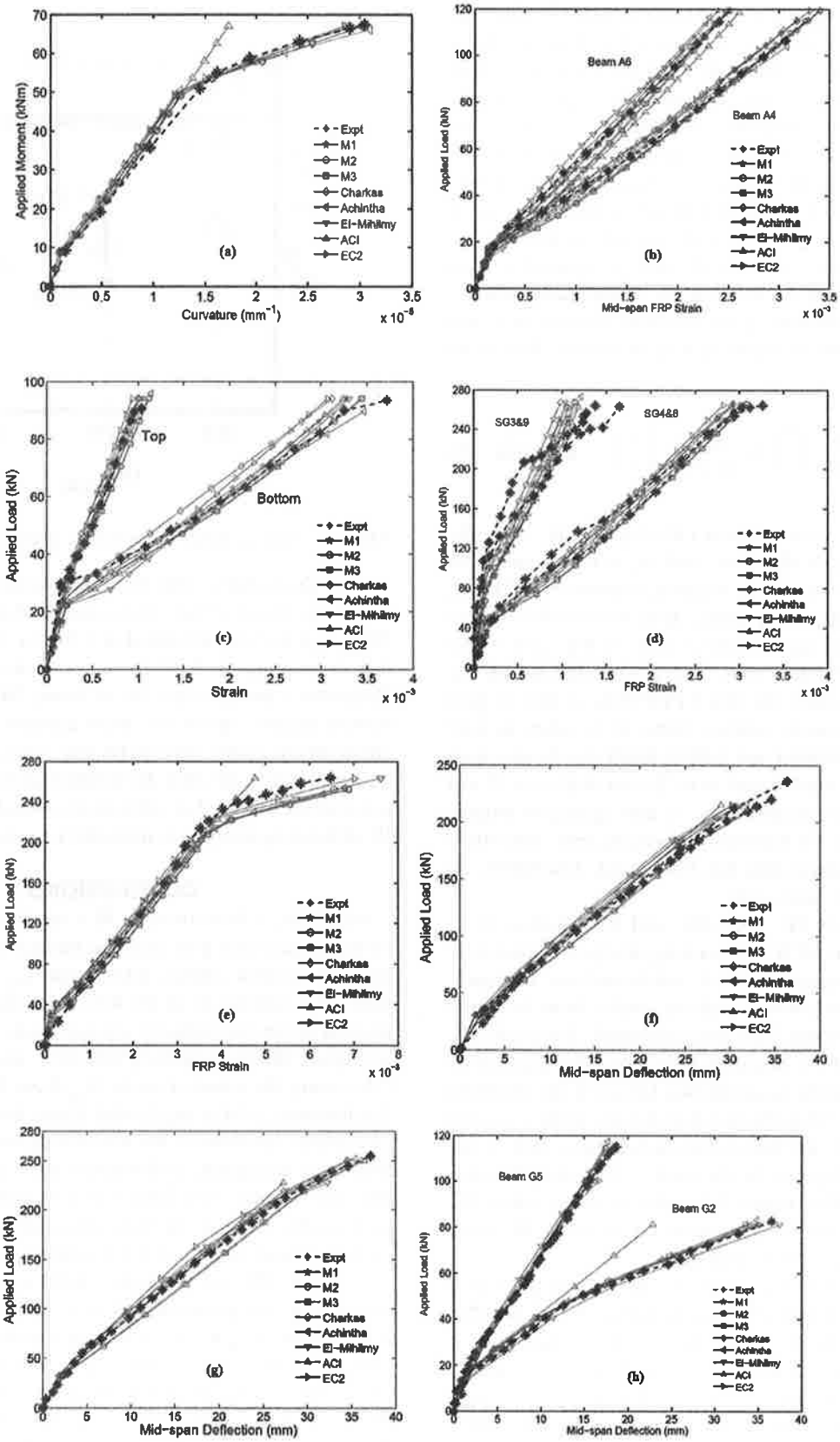

Fig. 9—Comparison of load-deformation relationships of different M-κ *models with experimental results: (a) Beam A3.1*[27]*; (b) Beams A4 and A6*[30]*; (c) Beam A*[28]*; (d) Beam CB4-2S*[26]*; (e) Beam CB4-2S (midspan)*[26]*; (f) Beams CB3-2S and CB4-2S*[26]*; (g) Beams CB5-3S*[26]*; and (h) Beams G2 and G5.*[25] *(Note: 1 kN = 0.225 kip; 1 kNm = 0.738 ft-kip; 1 mm = 0.039 in.)*

the FRP plate peeling off with concrete attached; therefore, the fracture is in the concrete. G_f associated with FRP-RC beam debonding is rarely assessed in experimental studies. The determination of G_f depends on many microstructural features such as size, shape, surface texture and location of the aggregate pieces, and also on the distribution of voids in

the mixture. Although there have been various experimental investigations, they were often associated with practical and conceptual difficulties. In PE debonding, a combination of normal and shear stress concentrations will be present in the vicinity of an existing interface crack, so the exact G_f would be a complicated mixed-mode fracture energy. A discussion of the nature and mode mixity of concrete fracture energy can be found in Reference 34, but is beyond the scope of this paper. The G_f used herein is the overall fracture energy, which by definition is the overall energy required to open a traction-free crack of unit length. Bažant and Emilie[35] reviewed a large number of the previous fracture tests and proposed an empirical expression to determine this value (Eq. (6)).

$$G_f = 0.0025\alpha_0\left(\frac{f'_c}{0.051}\right)^{0.46}\left(1+\frac{d_a}{11.27}\right)^{0.22}\left(\frac{w}{c}\right)^{-0.30} \text{ in N/mm} \quad (9)$$

where w/c is the water-cement ratio by weight; d_a is the maximum aggregate diameter; and α_0 takes 1 and 1.44 for rounded and crushed aggregates, respectively. The G_f value from Eq. (9) usually ranges from 0.07 to 0.17 N/mm (0.0048 and 0.0117 kip/ft). This is close to the value found in conventional Mode I tests, and is expected herein for PE debonding because the thin CFRP plate is free to peel away from the concrete surface. Here, G_f is taken as 0.07 and 0.15 N/mm (0.0048 and 0.0103 kip/ft) for beams with 10 mm (0.39 in) rounded, and 16 to 20 mm (0.63 to 0.79 in.) crushed aggregates, respectively. G_f and aggregate properties are commonly not reported for bending tests, but where possible, the reported data has been used. Elsewhere, an assumed value has been used.

The M-κ models M1, M2, M3, and the Charkas et al. model are used in GEBA debonding analysis respectively following the aforementioned whole-section treatment procedures. The debonding analysis results from Achintha and Burgoyne's model[12] are also compared. All results are shown in Fig. 11. A result that matches the predictions perfectly would predict a debonding failure at the observed load (so $P/P_{peak} = 1.0$ on the horizontal axis), at the expected location (given by the horizontal dashed line), and at the G_f value expected (given by the center of the error bars for the different models). Figure 11(d) shows a case where the Charkas et al. model has significant errors, while the other models all give very good agreement.

In general, the Charkas et al. model always predicts a much larger curtailment (L_p), which implies that debonding would occur at a higher load. This would be dangerous if used in design. It indicates that a straight line presentation of the partially cracked section oversimplifies the bending response, and is insufficient for GEBA use. For the other four models, the errors are generally within 10% variation of the load ($0.9P_{peak} < P < 1.1P_{peak}$) and the fracture energy (in the range of $0.9G_f$ to $1.1G_f$), if the debonding location varies within one cover depth ($(L_p - L_{rl})/c = \pm 1.0$) is allowed. The M1 and Achintha and Burgoyne's models agree best with the experimental results, and lie close to each other. In Fig. 11(g), however, Achintha and Burgoyne's model gives

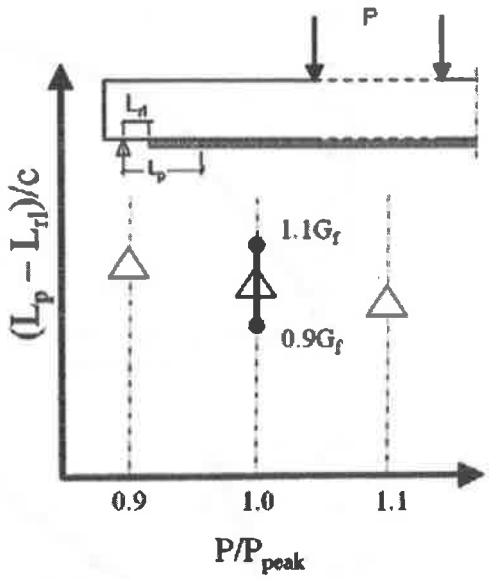

Fig. 10—Typical GEBA debonding analysis comparison.

a large discrepancy. The beam in question is the same as the beam shown in Fig. 11(h), except that it has much less FRP; it, however, debonded at a higher load. It is possible that decoupling the FRP force (as occurs in Achintha and Burgoyne's model) may be an issue. M3 gives well-correlated results, and is the most conservative (the bottom curve) in most cases (except for Fig. 11(e), (j), and (k) only), which demonstrates that the simplification adopted in M3 is reasonable. M2 is also satisfactory, which implies that the PE debonding analysis is insensitive to section nonlinearity.

CONCLUSIONS

Generally, a Branson-type M-κ model with modification to incorporate the post-yielding behaviors suffices to estimate an accurate energy release rate G_R. The M-κ models should be continuous at the first crack and first yield state, and curved in the partially cracked state. It should be able to capture the post-yielding behavior, which is essential in calculating the external work W_{ext} done during debonding. Furthermore, a M-κ model that treats the FRP-RC section as a whole can remove the uncertainty brought in from the FRP force decoupling and simplify the section analysis. The M1 and Achintha and Burgoyne's models have shown the best accuracy, while M3 has demonstrated a good match with experiments (although it is a little conservative in some cases). The M1 and Achintha and Burgoyne's models are complex in computation, whereas M3 is straightforward. These should be considered first for use in GEBA debonding analysis. There is very little experimental data to calibrate the moment-curvature relationship in a FRP-strengthened RC beam in the partially cracked state, however. Because this is the critical region when considering FRP debonding, the precision of the M-κ curve to be used is still open to some questions.

AUTHOR BIOS

Garfield X. Guan *is an Engineering Consultant in Hong Kong and China. He received his BEng in civil engineering from the University of Hong Kong, Pokfulam, Hong Kong, and his PhD from University of Cambridge,*

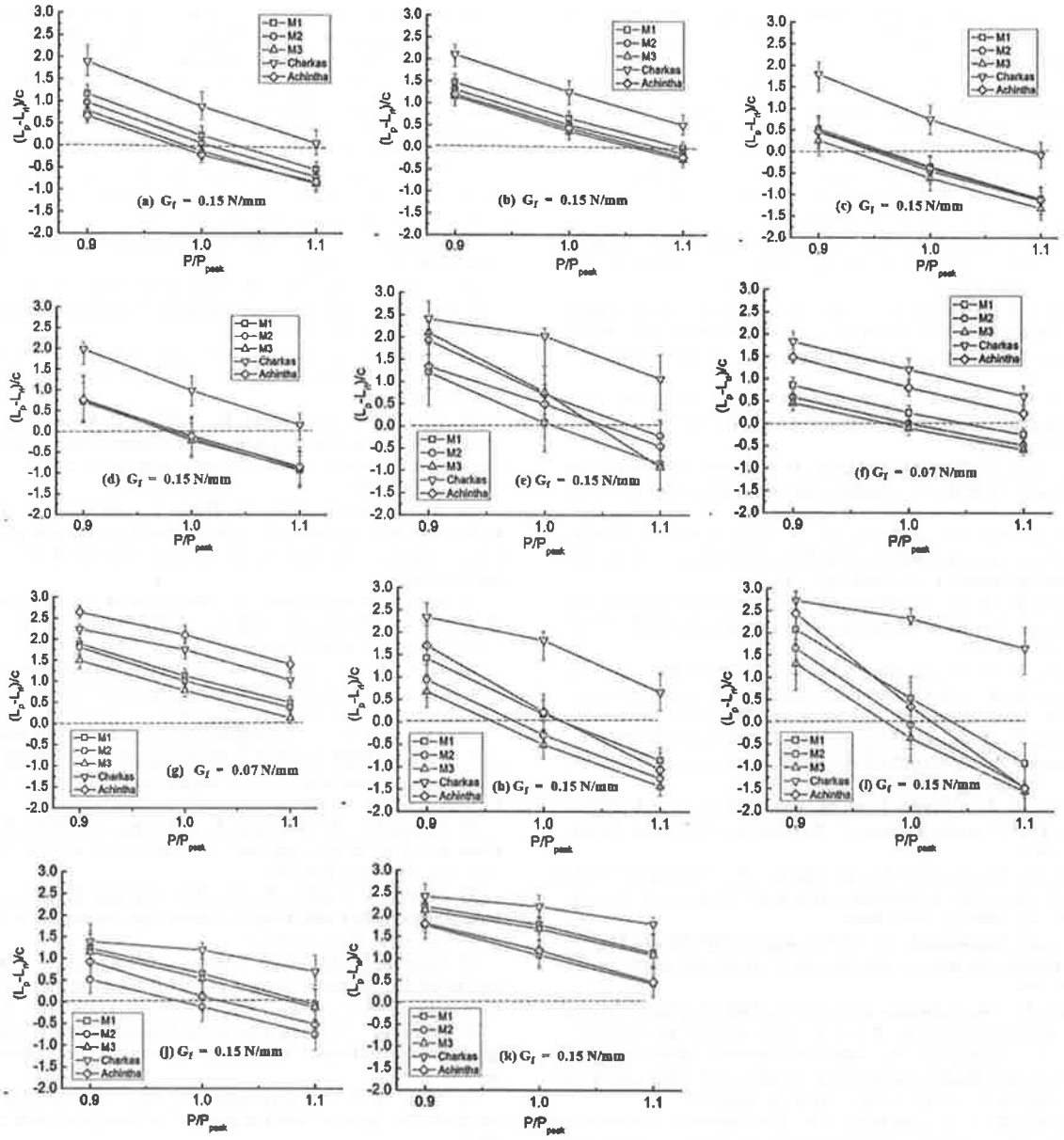

Fig. 11—Comparison of GEBA debonding analysis results with different M-κ *models against experiments: (a) Beam AF2[29]; (b) Beam AF3[29]; (c) Beam CF2-1[29]; (d) Beam CF3-1[29]; (e) Beam CF4-1[29]; (f) Beam A4[30]; (g) Beam A5[30]; (h) Beams F5 and F6[31]; (i) Beams F9 and F10[31]; (j) Beam A1100[32]; and (k) Beam A1150.[32] (Note: 1 N/mm = 0.0685 kip/ft.)*

Cambridge, UK. His research interests include reinforced concrete structure retrofitting, concrete fracture mechanics, and seismic engineering.

Chris J. Burgoyne *is Head of the Structures Group at the University of Cambridge. He has performed extensive research on the use of advanced fibers in a variety of civil, structural, and marine applications. He was a founding member of ACI Committee 440, Fiber-Reinforced Polymer Reinforcement.*

NOTATION

b, h, d, c = width, depth, effective depth, and concrete cover thickness of a beam, respectively
E_c = Young's modulus of concrete
F_{cc}, F_{cf}, F_{sc}, F_{st}, F_p = resultant force of concrete in compression, concrete in tension, compression steel, tension steel, and FRP retrofitting plate, respectively
$F_{p\text{-}RL}$, $F_{p\text{-}FB}$ = real and fully bonded FRP force
f_c' = concrete cylindrical strength
f_y = yield stress of tension steel
L_{rl} = curtailment length (distance from FRP plate end to support)
L_{shear} = shear span of FRP-RC beam
M_{cr}, M_y, M_{ult} = first cracking moment, yielding moment, and ultimate moment capacity, respectively
M_{fc}, M_{nc} = moment of fully cracked section and uncracked section, respectively
P_{peak} = experimental peak (debonding) load
t_p, t_a = thickness of FRP plate and adhesive layer
ε_s, ε_{sc}, ε_f, ε_1, ε_2 = strains at tension steel, compression steel, FRP plate, and top and bottom concrete fibers, respectively
κ_{cr}, κ_y, κ_{ult} = curvature of RC beam section at first cracking, at first yielding of tension steel, and at ultimate state, respectively
ρ_s, ρ_f = tension steel ratio $A_s/(bd)$ and FRP ratio $A_f/(bd)$

REFERENCES

1. Achintha, P. M. M., "Fracture Analysis of Debonding Mechanism for FRP Plates," PhD thesis, Department of Engineering, University of Cambridge, UK, 2009.

2. Smith, S. T., and Teng, J. G., "FRP-Strengthened RC Beams. I: Review of Debonding Strength Models," *Engineering Structures*, V. 24, No. 4, 2002, pp. 385-395.

3. Buyukozturk, O.; Gunes, O.; and Karaca, E., "Progress on Understanding Debonding Problems in Reinforced Concrete and Steel Members Strengthened with FRP Composites," *Construction & Building Materials*, V. 18, No. 1, 2004, pp. 1-19.

4. Aprile, A.; Spacone, E.; and Limkatanyu, S., "Role of Bond in RC Beams Strengthened with Steel and FRP Plates," *Journal of Structural Engineering*, ASCE, V. 127, No. 12, 2001, pp. 1445-1452.

5. Hamoush, S. A., and Ahmad, S. H., "Debonding of Steel Plate-Strengthened Concrete Beams," *Journal of Structural Engineering*, ASCE, V. 116, No. 2, 1990, pp. 356-371.

6. Davalos, J. F.; Kodkani, S. S.; and Ray, I., "Fracture Mechanics Method for Model-I Fracture Evaluation of FRP Bonded to Concrete Substrates," *Journal of Materials in Civil Engineering*, ASCE, V. 18, No. 5, 2006, pp. 732-742.

7. Taljsten, B., "Strengthening of Concrete Prisms Using the Plate Bonding Technique," *International Journal of Fracture Mechanics*, V. 82, No. 3, 1996, pp. 253-266.

8. Wu, Y.; Zhou, Z.; Yang, Q.; and Chen, W., "On Shear Bond Strength of FRP-Concrete Structures," *Engineering Structures*, V. 32, 2010, pp. 897-905.

9. Yang, Z. J.; Chen, J. F.; and Froverbs, D., "Finite Element Modeling of Concrete Cover Separation Failure in FEP Plated RC Beams," *Construction & Building Materials*, V. 17, 2003, pp. 3-13.

10. Achintha, P. M. M., and Burgoyne, C. J., "Fracture Mechanics of Plate Debonding," *Journal of Composites for Construction*, ASCE, V. 12, No. 4, 2008, pp. 396-404.

11. Achintha, P. M. M., and Burgoyne, C. J., "Moment-Curvature and Strain Energy of Beams with External Fiber-Reinforced Polymer Reinforcement," *ACI Structural Journal*, V. 106, No. 1, Jan.-Feb. 2009, pp. 20-29.

12. Achintha, P. M. M., and Burgoyne, C. J., "Fracture Mechanics of Plate Debonding: Validation against Experiment," *Construction & Building Materials*, V. 25, 2011, pp. 2961-2971.

13. Burgoyne, C. J.; Achintha, P. M. M.; and Guan, G. X., "A Fracture Approach for FRP-Concrete Structures," ACI Spring Convention, Minneapolis, MN, 2012.

14. Gunes, O.; Buyukozturk, O.; and Karaca, E., "A Fracture-Based Model for FRP Debonding in Strengthened Beams," *Engineering Fracture Mechanics*, V. 76, 2009, pp. 1897-1909.

15. Au, C., and Buyukozturk, O., "Debonding of FRP Plated Concrete: A Tri-Layer Fracture Treatment," *Engineering Fracture Mechanics*, V. 73, 2006, pp. 348-365.

16. Taljsten, B., "Strengthening of Beams by Plate Bonding," *Journal of Materials in Civil Engineering*, ASCE, V. 9, No. 4, 1997, pp. 206-212.

17. Sakai, K., and Kakuta, Y., "Moment-Curvature Relationships of Reinforced Concrete Members Subjected to Combined Bending and Axial Force," *ACI Journal*, V. 77, No. 3, Mar. 1980, pp. 189-194.

18. Faruqi, M.; Wu, C. C.; and Benson, F., "Development of Deflection Equations Using Moment-Curvature Relationships for Reinforced Concrete Beams Strengthened with Fibre-Reinforced Polymer (FRP) Plates," *Magazine of Concrete Research*, V. 55, No. 6, 2003, pp. 549-557.

19. El Mihilmy, M., and Tedesco, J. W., "Deflection of Reinforced Concrete Beams Strengthened with Fiber-Reinforced Polymer Plates," *ACI Structural Journal*, V. 97, No. 5, Sept.-Oct. 2000, pp. 679-688.

20. Charkas, H.; Rasheed, H. A.; and Melhem, H., "Rigorous Procedure for Calculating Deflections of Fiber-Reinforced Polymer-Strengthened Reinforced Concrete Beams," *ACI Structural Journal*, V. 100, No. 4, July-Aug. 2003, pp. 529-539.

21. Mota, C.; Alminar, S.; and Svecova, D., "Critical Review of Deflection Formulas for FRP-RC Members," *Journal of Composites for Construction*, ASCE, V. 10, No. 3, 2006, pp. 183-194.

22. Branson, D. E., *Deformation of Concrete Structures*, McGraw-Hill, New York, 1977, 576 pp.

23. ACI Committee 318, "Building Code Requirements for Structural Concrete (ACI 318-08) and Commentary," American Concrete Institute, Farmington Hills, MI, 2008, 473 pp.

24. Hognestad, E.; Hanson, N. W.; and McHenry, D., "Concrete Stress Distribution in Ultimate Strength Design," *ACI Journal*, V. 52, No. 4, Apr. 1955, pp. 455-480.

25. Ross, C. A.; Jersome, D. M.; Tedesco, J. W.; and Hughes, M. L., "Strengthening of Reinforced Concrete Beams with Externally Bonded Composite Laminates," *ACI Structural Journal*, V. 96, No. 2, Mar.-Apr. 1999, pp. 212-220.

26. Alagusundaramoorthy, P.; Harik, E.; and Choo, C. C., "Flexural Behavior of R/C Beams with Carbon Fibre Reinforced Polymer Sheets or Fabric," *Journal of Composites for Construction*, ASCE, V. 7, No. 4, 2003, pp. 292-301.

27. Spadea, G.; Bencardino, F.; and Swamy, R. N., "Structural Behavior of Composite RC Beams with Externally Bonded CFRP," *Journal of Composites for Construction*, V. 2, No. 3, 1998, pp. 132-137.

28. Li, A.; Assih, J.; and Delmas, Y., "Shear Strengthening of RC Beams with Externally Bonded CFRP Sheets," *Journal of Structural Engineering*, ASCE, V. 127, No. 4, 2001, pp. 374-380.

29. Ahmed, O. A. F., "Strengthening of RC Beams by Means of Externally Bonded CFRP Laminates. Improved Model for Plate-End Shear," PhD thesis, Department of Civil Engineering, Catholicke University of Leuven, Belgium, 2000.

30. Arduini, M.; Di-Tommaso, A.; and Nanni, A., "Brittle Failure in FRP Plate and Sheet Bonded Beams," *ACI Structural Journal*, V. 94, No. 4, July-Aug. 1997, pp. 363-370.

31. Fanning, P. J., and Kelly, O., 2001, "Ultimate Response of RC Beams Strengthened with CFRP Plates," *Journal of Composites for Construction*, ASCE, V. 5, No. 2, pp. 122-127.

32. Nguyen, D. M.; Chan, T. K.; and Cheong, H. K., "Brittle Failure and Bond Development Length of CFRP-Concrete Beams," *Journal of Composites for Construction*, ASCE, V. 5, No. 1, 2001, pp. 12-17.

33. Eurocode 2, "Design of Concrete Structures. Part 1-1: General Rules and Rules for Buildings," British Standards Institution, London, UK, 2004, pp. 129-130.

34. Shah, S. P., and Carpinteri, A., eds., "Fracture Mechanics Test Methods for Concrete," *RILEM Report* 5, Chapman & Hall, London, UK, 1991.

35. Bažant, Z. P., and Emilie, B. G., "Statistical Prediction of Fracture Parameters of Concrete and Implications for Choice of Testing Standard," *Cement and Concrete Research*, V. 32, 2002, pp. 529-556.